Interface Engineering Catalytic Graphene for Smart Colorimetric Biosensing

Meng Liu, Huimin Zhao, Shuo Chen, Hongtao Yu, and Xie Quan*

School of Environmental Science and Technology, Key Laboratory of Industrial Ecology and Environmental Engineering (Ministry of Education, China), Dalian University of Technology, Dalian, 116024, China

ABSTRACT

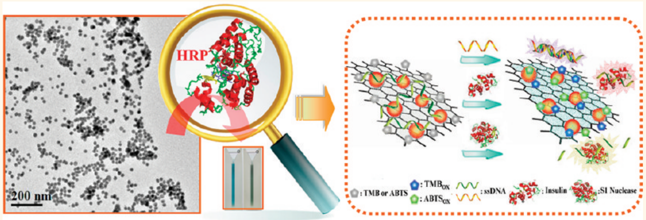

Herein a hybrid catalyst consisting of "naked" Au-NPs *in situ* grown on graphene sheets is engineered, which exhibits a synergetic effect in mimicking peroxidase at its interface, although free Au-NPs or graphene alone has very little activity. What is more, one of the unique features of our synergetic catalyst is that its interface can be reversibly switched from "inactive" to "active" upon treatment with different ssDNA species in solution, thus providing a powerful and versatile basis for designing graphene/DNA-based label-free colorimetric biosensors. Compared with other signal transduction modes in traditional graphene/aptamer-based systems, our novel signaling strategy not only avoids any labeling or modification procedures but also reduces the background signal due to the "off—on" switching mode during the sensing. Furthermore, this facile and general approach can be applicable to the other extended graphene/aptamer-based systems for colorimetric detection of a wide range of analytes. We envision that the tunable graphene-based smart interface could find potential applications in the development of biocatalysis, bioassays, and smart material devices in the future.

KEYWORDS: aptamer · colorimetric · catalytic · graphene · smart interface

As an atomically thick sheet of nanocarbon, two-dimensional graphene-based material (graphene and its derivatives) has recently emerged as a rising star in the areas of physics, chemistry, and materials science.[1,2] As noted, benefiting from their amazing electronic, optical, and mechanical properties,[3−5] graphenes appear to be ideal signal transducing elements for the construction of sensors based on various transduction modes.[6−15] In particular, the π-rich conjugation surface domains enable graphenes to interact with biomolecular receptors through noncovalent or electrostatic interactions, especially with aptamers, a novel class of functional single-stranded DNA or RNA molecules (more recently, peptides) isolated by *in vitro* selection that can bind to diverse targets with high affinity and specificity,[16,17] thus opening new opportunities for designing aptamer-based platforms in biosensing. In general, current graphene/aptamer-based sensors require covalent coupling of commercially available dye,[18−21] luminescent nanocrystals,[22,23] conjugated polymers,[24] or electroactive tags[25] in the biorecognition system to serve as the signal reporter. In addition, some modified "receptors" with functional groups (such as $-$SH,[26,27] $-$COOH,[28] or $-PO_3H$[29]) are even needed to fabricate a sensing surface that is sensitive to the target invasion. However, either a labeling or a modification process will not only result in laborious and expensive synthetic or purification steps, thus inducing high cost of operation in the applications, but also lead to significant loss in affinity or specificity of the receptor compared with its unmodified analogue,[30,31] thereby reducing the sensitivity or selectivity during the sensing.

To overcome these limitations, efforts have focused on the development of graphene/aptamer-based label-free sensors. One is the fluorescent sensor by means of either specific binding dye[32,33] or rational synthetic conjugated oligoelectrolyte;[34] the other is the electrochemical sensor taking advantage of the π-stacking interactions between nucleotide bases and the graphene surface,[35,36] the signal of which could be changed in the presence of targets. Despite these achievements, few can match or exceed the sensitivity or selectivity of labeled sensors. Moreover, developing a facile approach for the design of graphene/aptamer-based sensors in terms of employing unlabeled or unmodified aptamer and extending this method to other aptamers remain great challenges. In this respect, it is highly desirable to explore other universal signaling strategies to meet these challenges.

* Address correspondence to quanxie@dlut.edu.cn.

Received for review December 16, 2011 and accepted March 23, 2012.

10.1021/nn3010922

Herein, we report the engineering of a tunable smart interface at a synergistic graphene-based catalyst that exhibits dynamic and reversible changes in interfacial property in response to biological stimuli, thus making it a promising and attractive candidate for constructing label-free colorimetric biosensors. In such an approach, catalytic graphene serves as a signal reporter that converts the recognition reaction into a colorimetric signal. The working principle is illustrated in Scheme 1. We demonstrate that graphene-based hybrids consisting of "naked" Au nanoparticles (NPs) supported on graphene sheets possess excellent synergistic peroxidase-like activity at their interfaces, as indicated by a typical color reaction in the presence of peroxidase substrates, although graphene or Au-NPs alone has little activity. However, the addition of aptamer or single-stranded DNA (ssDNA) can prevent the peroxidase substrates from diffusing and binding to the active interface that is essential for the catalytic reaction due to the formation of self-assembled biocomposites, thereby allowing the catalytic activity to be switched "off". Conversely, the introduction of targets (such as specific DNA sequence, insulin molecule, or S1 nuclease) will induce conformational change or cleavage in the aptamer chains, leading to the weak binding affinity between the aptamer/target complex and the graphene/Au-NP surface. As a result, the "inactive" interface originally passivated or protected by the aptamer will become active, which can switch "on" the catalytic reaction, thus producing color changes in relation to target amounts. On the basis of the tunable smart interface of catalytic graphene, one may be able to design a label-free colorimetric platform toward sequence-specific DNA sensing, protein–aptamer interaction study, and DNA cleavage monitoring.

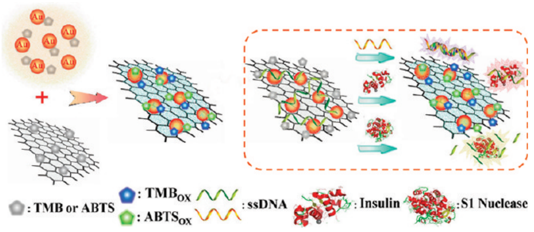

Scheme 1. Schematic illustration of a versatile and label-free colorimetric biosensing platform based on the tunable smart interface of catalytic graphene/Au-NP hybrid.

RESULTS AND DISCUSSION

To demonstrate the feasibility of our protocol, we first synthesized the graphene/Au-NP hybrid in solution by a one-step hydrothermal reaction of $HAuCl_4$ and graphene oxide (GO, Figure 1A) at 180 °C. During this process, the $HAuCl_4$ precursor was directly reduced to Au-NPs and then anchored to the graphene surface mainly through the defects and oxygen functional groups.[37] Note that the resultant hybrid can form well-dispersed aqueous colloids owing to the residual oxygen-containing groups on the graphene surface,[38] which could be beneficial to its potential application in bioassays. Figure 1B,C shows typical transmission electron microscopy (TEM) images of the as-prepared hybrid, in which Au-NPs were uniformly deposited on

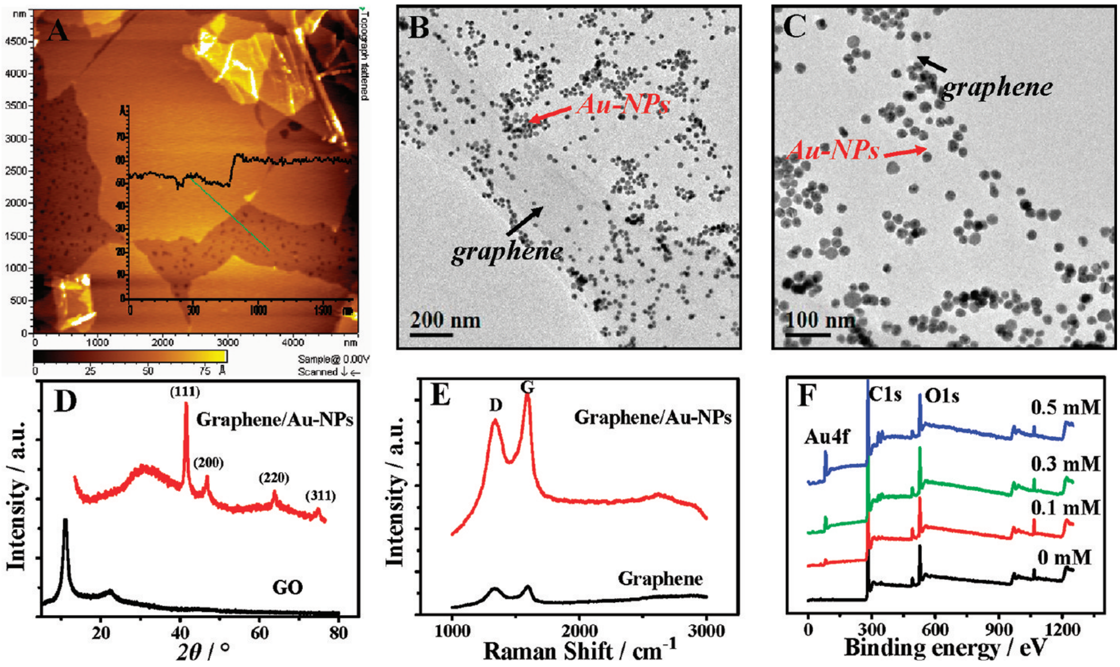

Figure 1. (A) Typical AFM image and height profile of GO on freshly cleaved mica substrate. (B,C) TEM images of Au-NPs *in situ* grown on graphene sheets under different magnifications. (D) XRD spectra of GO and graphene/Au-NP hybrid. (E) Raman spectra of graphene and graphene/Au-NP hybrid. (F) XPS spectra of the pure graphene and graphene/Au-NP hybrid with different Au contents.

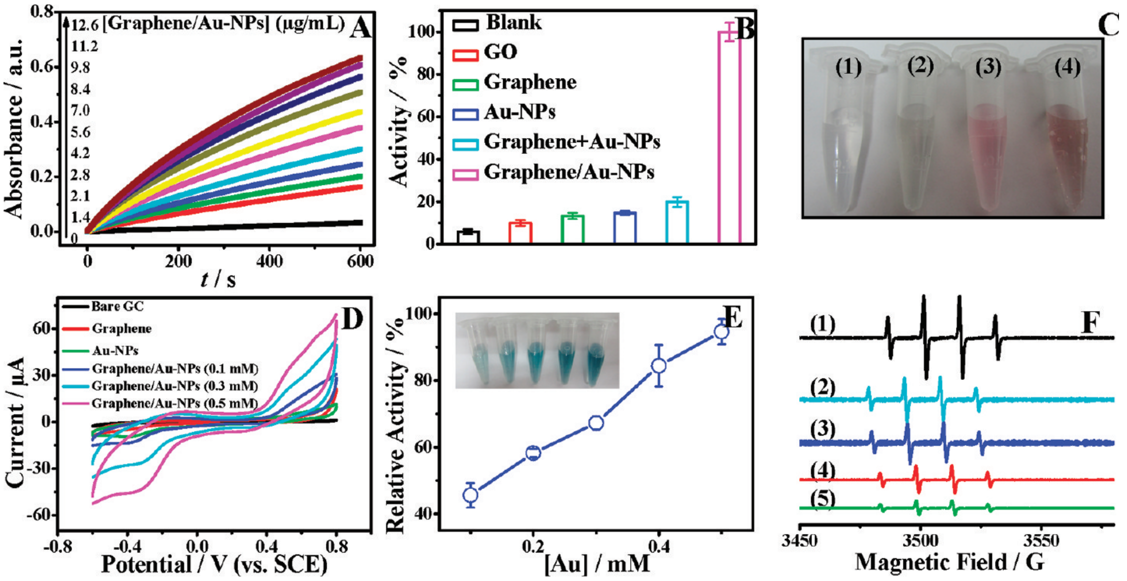

Figure 2. (A) Time-dependent absorbance changes at 652 nm of TMB reaction solutions catalyzed by graphene/Au-NPs at various levels. (B) Comparison of catalytic activities of GO, graphene, Au-NPs, graphene/Au-NPs, and physical mixtures of graphene with Au-NPs under the same condition. The maximum point was set as 100%. (C) Observation of H_2O_2 decomposition without catalyst (1) and catalyzed by graphene (2), Au-NPs (3), and graphene/Au-NPs (4) in water. (D) Cyclic voltammetry of a bare GC, GC/graphene, GC/Au-NPs, and GC/graphene/Au-NP hybrids (with various Au contents) in N_2-saturated PBS solution (0.1 M, pH 7.4) in the presence of 1 mM H_2O_2. Scan rate: 50 mV/s. The catalyst loading was 1.5 μg. (E) Relative activities of graphene/Au-NP composites with various Au content (from left to right: 0.1, 0.2, 0.3, 0.4, 0.5 mM). (F) DMPO spin-trapping ESR spectra of H_2O_2/UV system recorded in aqueous dispersion with (1) 0 μg/mL; (2) 5 μg/mL; (3) 10 μg/mL; (4) 15 μg/mL; and (5) 20 μg/mL graphene/Au-NP hybrid. Experiments were carried out in 20 mM phosphate buffer (pH 4.0) containing 6 μg/mL catalyst, 50.4 mM H_2O_2, and 0.28 mM TMB, unless otherwise stated.

the graphene surface with a narrow size distribution (22.1 ± 1.5 nm, Figure S1 in Supporting Information). In strong contrast, free Au-NPs prepared by the same method without GO possessed a broad size distribution (23.9 ± 4.9 nm, Figure S2), highlighting the role of GO as an efficient support to disperse and stabilize Au-NPs, similar to the results observed in Pt (or Pd)-NP/GO composites.[39,40] The high-resolution TEM image showed that the lattice spacing of the Au-NPs was about 2.34 Å (Figure S3), corresponding to the distance of (111) lattice spacing of the Au crystal, and the X-ray diffraction (XRD) pattern further suggested the crystalline nature of Au-NPs grown on the graphene surface (Figure 1D). Energy-dispersive spectroscopy (EDS) spectrum also confirmed the formation of Au-NPs on graphene sheets (Figure S4). Raman spectroscopy in Figure 1E revealed the Raman signal enhancement for graphene/Au-NP hybrids, which was consistent with the surface-enhanced Raman scattering effect previously reported in dendritic Au/graphene structures,[41] indicating the interaction of Au-NPs with graphene. The formation of graphene/Au-NP hybrids was further characterized by X-ray photoelectron spectroscopy (XPS). Figure 1F shows the increased Au 4f signal in the resulting hybrids with increasing Au content, indicating that Au-NPs were successfully assembled on the graphene surface.

In the following, we devoted to assess the interfacial property of the catalyst. It was observed that graphene/Au-NPs were capable of catalyzing the oxidation of peroxidase substrates 3,3′,5,5′,-tetramethylbenzidine (TMB) and 2,2-azinobis(3-ethylbenzothiazoline-6-sulfonic acid) (ABTS) by H_2O_2 to produce a blue color (typical absorbance at 652 nm) and green color (typical absorbance at 410 nm), respectively (Figure S5), and the color reaction (for TMB) could even be quenched by the addition of H_2SO_4 (Figure S6). In contrast, no obvious reaction occurred in the absence of catalyst (Figure S7), suggesting the peroxidase-like activity of the as-prepared hybrid. Figure 2A indicates time-dependent absorbance changes (at 652 nm) against different concentrations of graphene/Au-NPs. With increasing catalyst concentration, the catalytic rate was greatly improved. Furthermore, like other nanomaterial-based peroxidase mimics,[42−45] its activity was also dependent on pH, temperature, and H_2O_2 concentration (Figure S8 and S9). As noted, in contrast to that found for natural peroxidase and Fe_3O_4 nanoparticles,[42] no inhibition effect was observed at high H_2O_2 concentration (Figure S9). To compare the activity of graphene/Au-NP hybrids and horseradish peroxidase (HRP), typical Michaelis−Menten curves were obtained in a certain range of H_2O_2 or TMB concentrations. As expected, the calculated values of reaction rate (v_{max}) for our catalyst with TMB and H_2O_2 as substrates were about 1.3 and 1.4 times higher than those for HRP (Table 1), indicating the higher catalytic activity of graphene/Au-NP hybrids. Meanwhile, the catalyst possessed larger Michaelis constant (K_m) than that for HRP, consistent with the

TABLE 1. Comparison of the Kinetic Parameters between Graphene/Au-NPs and HRP[a]

	substrate	K_m (mM)	v_{max} (10^{-8} M/s)
hybrid	H_2O_2	274.22	25.6 ± 5.8
hybrid	TMB	0.29	5.6 ± 0.7
HRP	H_2O_2	6.36	18.8 ± 4.6
HRP	TMB	0.041	4.3 ± 0.8

[a] The apparent kinetic parameters were calculated based on Michaelis–Menten function: $\nu = v_{max}[S]/(K_m + [S])$, where K_m was the Michaelis constant; v_{max} was the maximal reaction velocity, and [S] was the substrate concentration.

result that a higher H_2O_2 concentration was necessary to obtain a higher activity. We ascribed the enhanced catalytic activity to the positive synergetic coupling effect that occurred at the interface of inert graphene and poorly active Au-NPs, as can be deduced from Figure 2B that either graphene alone or free Au-NPs (like these grown on the graphene surface but with relative broad size distribution, Figure S2) exhibited little peroxidase-like activity toward TMB (also see Figure S10). Remarkably, the simple physical mixtures of Au-NPs with graphene also showed performance inferior to that of Au-NPs grown on graphene, suggesting that the intimate binding in the hybrid was required to impart the synergetic effect between graphene and Au-NPs, similar to the observation in a synergetic catalyst of Co_3O_4/graphene reported by Liang *et al.*[46] Very recently, Guo *et al.*[47] demonstrated that the graphene–hemin composite prepared by a wet-chemical method *via* π–π interaction also had the intrinsic peroxidase-like activity, whereas its catalytic activity was lower than that of hemin itself, further confirming the importance of intimate interfacial interactions in a supported system to the enhanced catalysis. In fact, the synergistic effect in the graphene/Au-NP catalyst can also be visually observed through the decomposition of H_2O_2 even in the absence of TMB, as indicated in Figure 2C that a lot of bubbles were formed after incubating the graphene/Au-NP hybrid with H_2O_2, similar to the behavior of natural catalase.[44] On the contrary, no bubbles were observed in free Au-NPs or the pure graphene sample. In order to better investigate the synergistic effect in graphene-supported catalyst systems, we compared the electrocatalytic behavior of the graphene/Au-NPs with graphene or Au-NPs alone toward H_2O_2 reduction. In contrast to the poor response of graphene or the Au-NP-modified electrode, the graphene/Au-NP electrode exhibited a well-defined and enhanced reduction peak around −0.4 V (Figure 2D), which was indicative of a synergistic effect of graphene and Au-NPs on the improvement of catalytic performance. Furthermore, one observed that the electrocatalytic activity increased with increasing Au content in graphene/Au-NP hybrids, implying the important role of Au species at the interfaces for enhanced catalysis. This assertion was further confirmed by the result presented in Figure 2E that an obvious increase in the peroxidase-like activity was accompanied by an increase of the Au content in the catalyst (from 0.1 to 0.5 mM).

Theoretical investigations demonstrated the significance of carbonyl or carboxyl groups in modulating the band gap in graphene, facilitating the electrocatalytic reduction of adsorbed H_2O_2,[48,49] which also supported the experimental observation that carboxylated carbon-based materials possessed the intrinsic peroxidase-like activity.[43,45] Together with the fact that Au-NPs had an important effect on the enhanced catalysis of reduced graphene, deduced from the results from both peroxidase-like activity and electrocatalytic activity studies, we attempted to gain more insight into the origin of the synergetic catalytic behaviors of the Au-embedded graphene system. (1) It was proposed that the oxygenated functional groups and carbon vacancy defects on the GO surface played an essential role in the bonding formation of graphene–metal contacts depending on the interaction between π orbitals in graphene and d orbitals in metals.[39–41,50] In view of the enhanced Raman signal in the Au-embedded graphene system, as shown in Figure 1E, we inferred that the strong covalent interfacing of Au-NPs with reduced graphene originated from attractive interaction between carbon 2p and Au 5d orbitals around the carbon vacancy and defect,[41,51] which would be favorable to H_2O_2 adsorption, in turn drastically affecting the H_2O_2 reduction reaction. In fact, this was a crucial step for electrocatalytic reduction of H_2O_2.[49] Furthermore, EPR spectra in Figure 2F indicated that the signal intensity of •OH radicals decreased sharply with the addition of a graphene/Au-NP hybrid in the H_2O_2/UV/DMPO system, suggesting that a large amount of H_2O_2 or •OH radicals adsorbed on the catalyst (especially in the interfacial region[51]) escaped from EPR detection.[52] (2) Calculations based on density functional theory predicted that the chemical interaction at the graphene–metal interface could modify the electronic structure and Fermi level in graphene, engendering doping with either electrons or holes driven by the work function difference and band gap opening.[53,54] To explore the doping effect, Raman spectra were carried out at room temperature. In Figure 3A, three main peaks were assigned to the graphene sample: the D-band (1339 cm^{-1}), G-band (1591 cm^{-1}), and 2D-band (2662 cm^{-1}). Upon doping, one observed that the position of the G-band and 2D-band up-shifted and down-shifted, respectively, indicating the robust covalent interfacing of Au with graphene and the n-type doping of graphene.[55–57] Remarkably, the sample with the highest Au content showed the largest shift. Note that the 2D-band can be deconvoluted at least two peaks due to the presence of multilayer graphene. The high-resolution C 1s XPS spectra also confirmed the n-type doping effect. In Figure 3B, the main C 1s peak related to pure sp^2 C–C bonds shifted to higher binding energy (284.28 eV) as compared with pure graphene (283.99 eV), behaving as n-type doping,[57,58] which contributed to an increase in charge carrier density and mobility at the graphene–metal interface,[54,59,60] thus accelerating the catalytic reactions in the presence of redox species.[43,61] It was notable that our results agreed with the theoretical calculation which suggested the enhanced catalytic activity in the Au-embedded graphene.[51,62] Taken together, originating from the synergetic effects between graphene and Au-NPs, the composite material indeed showed an excellent peroxidase-like activity at its interface, which would be suitable for a wide range of potential applications in catalysis and bioassays.

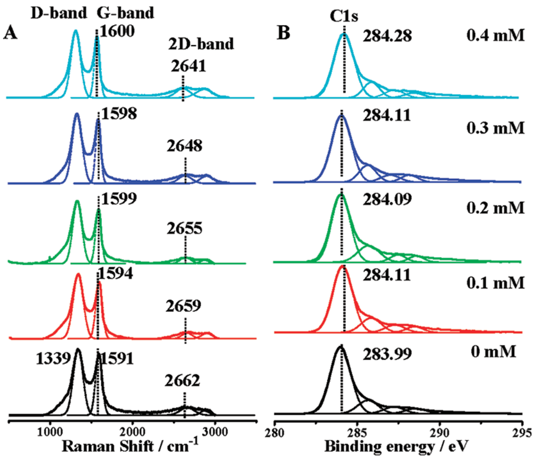

Figure 3. Evolution of the (A) G-band and 2D-band in Raman spectra, and (B) C 1s electrons in high-resolution XPS spectra upon doping for graphene.

One of the unique features of our synergetic catalyst was that its interface can be reversibly switched from "inactive" to "active" upon treatment with different ssDNA species in solution. As shown with a random ssDNA (P1: 29-mer, Table S1) as an example (Figure 4A), the interface became more inactive following treatment with P1. For instance, its catalytic activity remained less than 8% when the P1 concentration reached 1.1 μM. Considering the strong $\pi-\pi$ interactions between the nucleobases and the graphene surface,[63] it was expected that ssDNA can be easily adsorbed onto the catalytic graphene. Furthermore, we noted that ssDNA can easily stick to Au-NPs, benefiting from its flexible structure.[64] Study on the relative activity of the graphene/Au-NP hybrids with lower Au-NP density (prepared by increasing the initial GO concentration to 0.08 mg/mL) following ssDNA treatment would allow us to look into the role of Au-NPs/ssDNA interactions. As shown in Figure 4B, a comparison of the relative activities of the graphene/Au-NP catalyst with different Au-NP densities upon addition of 0.8 μM ssDNA indicated the efficient deactivation results independent of Au-NP density, elucidating the important role of interactions between Au-NPs and ssDNA. That is, the presence of ssDNA can be exposed to both the graphene surface and Au-NPs despite the fact that the density of Au-NPs on the graphene surface was relatively small, which would

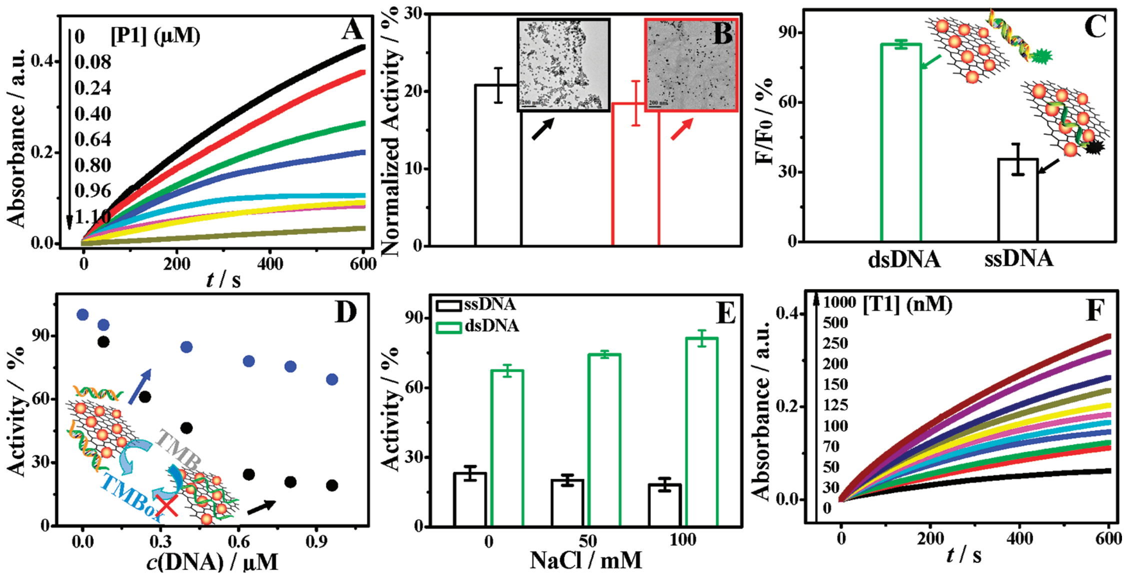

Figure 4. (A) Time-dependent absorbance changes at 652 nm of TMB reaction solutions catalyzed by graphene/Au-NPs in the presence of different amounts of ssDNA (P1). (B) Comparison of the activity of graphene/Au-NPs with different Au-NP densities after treatment with 0.8 μM ssDNA. Note that the data were normalized to highlight the decrease in activity. (C) Comparison of FL retention ratio of FAM-labeled P1 and dsDNA after incubated with graphene/Au-NPs for 20 min. (D) Catalytic activity of graphene/Au-NPs in the presence of various concentrations of P1 (black dots) or dsDNA (blue dots). (E) Effects of salt concentration (0, 50, and 100 mM) on the activity of graphene/Au-NPs induced by ssDNA (P1) or dsDNA. (F) Time-dependent absorbance changes at 652 nm with varying concentrations of T1. The concentration of P1 was fixed at 1 μM. Experiments were carried out in 20 mM phosphate buffer (pH 4.0) containing 8 μg/mL catalyst, 30 mM H_2O_2, and 0.5 mM TMB, unless otherwise stated.

effectively prevent the peroxidase substrates from diffusing and binding to the graphene/Au-NP interface, especially the active sites that were essential for the reaction, thus allowing the catalytic reaction to be switched off. To further confirm this scenario, a kinetics study was carried out to record the time-dependent fluorescence (FL) changes of FAM-labeled ssDNA (29-mer) after exposure to the catalyst (Figure S11). One observed that the FL retention ratio was less than 35%; in other words, more than 65% of the FL was quenched as a result of the energy or electron transfer from fluorophore to graphene (Figure 4C),[65] indicating the formation of the self-assembled graphene/Au-NPs/ssDNA complex. Note that if sufficient "quenchers" were allowed, complete quenching efficiency can be achieved (Figure S11). Furthermore, we investigated the effect of double-stranded DNA (dsDNA) on the activity over our catalyst. Due to the stiffer structure of dsDNA, it was concluded that the binding interactions of the graphene-based composite with dsDNA were significantly weak (as also indicated by the negligible quenching effect in Figure S11). In this case, the addition of dsDNA was not able to block the accessibility of peroxidase substrates to the graphene/Au-NP interface, thereby rendering no striking inhibition effect on catalytic activity (Figure S12). As shown in Figure 4D, with increasing dsDNA concentration, the activity decreased very slowly compared to that for ssDNA. This evidence suggested that the inhibition effect in the ssDNA system could be related to the steric hindrance effect due to the formation of the graphene/Au-NPs/ssDNA complex. Given the fact that quite a few of the repeat units were in the dsDNA, the electrostatic interaction between a dsDNA and a positively charged TMB would be much stronger than that of a ssDNA and the TMB, which caused the formation of the dsDNA/TMB complex, thus resulting in the "false" inhibition effect on the catalytic activity.

To confirm our hypothesis, the effect of salt concentration on the activity of graphene/Au-NPs in the presence of ssDNA (P1) or dsDNA was investigated. It was well-known that the buffer ions can decrease the electrostatic layer of counterions, thus resulting in the screening of electrostatic attraction according to Debye–Hückel theory.[66] Therefore, the presence of salt was expected to weaken the electrostatic interaction between dsDNA and TMB. As shown in Figure 4E, a slight but distinct change in the catalytic activity was observed after addition of NaCl to the dsDNA system, as compared to that for the ssDNA system, thus suggesting that the dominant interaction in the dsDNA system was electrostatic, which further revealed the importance of graphene/ssDNA and Au-NPs/ssDNA interactions in the ssDNA system in determining the catalytic activity.

To eliminate the false-negative results in the dsDNA system, a negatively charged substrate, ABTS, was used instead of TMB. As expected, only a little reduction of the activity was observed when ABTS was added upon treatment with dsDNA (Figure S13). For example, the decreased activity was estimated to be 15%, in comparison with that of 31% in TMB reaction solutions. Therefore, the fact of the controllable interfacial properties of the nanocomposites suggests that these findings may, with further study, have potential applications in sensors, nanofluidics, smart devices, and switchable surfaces, which largely extends the application range of nanomaterial-based peroxidase mimics.[42−45] Furthermore, taking advantage of the DNA species-responsive interface of catalytic graphene, it was possible to develop a simple, homogeneous, and label-free colorimetric method to assay the conformational changes of ssDNA or aptamer in solution. As noted, despite the impressive progress in the construction of graphene-based biological or chemical sensors in various transduction modes, from optical transduction (such as surface-enhanced Raman spectroscopy, luminescence, and fluorescence)[10,11,18−25] to electrochemical transduction (such as amperometry, field-effect transistor, surface plasmon resonance, and photoelectrochemistry),[7−9,12−15,25,27−29,36] research efforts on the design of novel colorimetric sensors based on graphene or its composite are still rudimentary.[43,47]

To verify its potential applications, the catalytic graphene/Au-NP-based platform was first adopted for DNA hybridization analysis. As a proof-of-concept experiment, a random sequenced P1 was chosen as a probe. In the presence of 1 μM P1, the catalyst did not display apparent activity as can be deduced from the negligible color changes of substrate TMB, thus providing an excellent colorimetric sensing system with low background interference. In direct contrast, when P1 was first hybridized with its complementary target T1 to form a duplex, an obvious color signal was produced with the reaction time (Figure 4F). Meanwhile, the color intensity was indeed dependent on the concentration of T1, and the detection limit was calculated to be 11 nM based on the 3δ/slope rule (Figure S14). More importantly, this protocol can easily discriminate single-base mismatches in target DNA sequences with specific responses (Figure S15), making it a promising candidate for future single-nucleotide polymorphism (SNP) genotyping.[67]

To further explore its potential for practical application in bioassay, we applied the method to detect the 21-mer hepatitis C virus (HCV) DNA sequence in the media of blood serum (supplied by a hospital).[68] The results in Figure S16A showed that the catalytic activity of our catalyst (first treated with 1.4 μM HCV DNA probe) increased accordingly with the increasing concentrations of HCV-1b cDNA in the serum media. Furthermore, one observed that good recovery values can be obtained in measuring HCV-1b cDNA level in spiked serum media (Table S1), indicating that our method could be employed to detect DNA targets

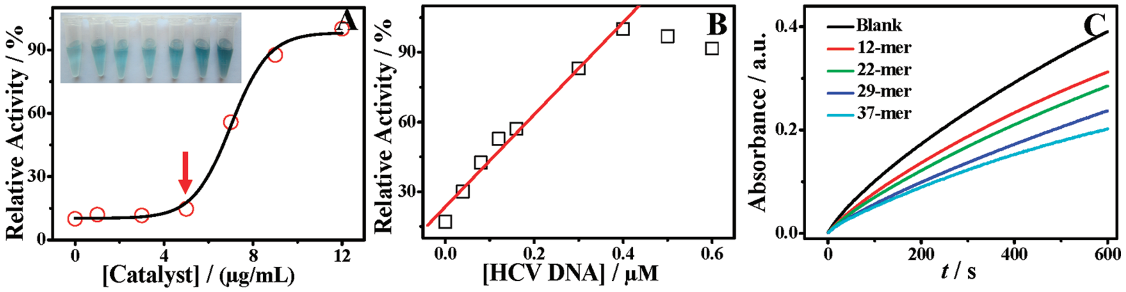

Figure 5. (A) Activities of graphene/Au-NPs with varying concentrations (from left to right: 0, 1, 3, 5, 7, 9, 12 μg/mL) in the presence of HCV cDNA sample (total final concentration of 1.0 μM, containing 0.4 μM HCV-1b cDNA). Note that the signal response in the absence of catalyst was a result from the catalysis of biological enzymes in serum. The maximum point was set as 100%. (B) Effects of HCV DNA probe concentration on the catalytic activity of graphene/Au-NPs (5 μg/mL) after treatment with HCV cDNA sample in serum media. (C) Time-dependent absorbance changes at 652 nm of TMB reaction solutions catalyzed by graphene/Au-NPs in the presence of 0.3 μM ssDNA with different lengths. Experiments were carried out in 20 mM phosphate buffer (pH 4.0) using 8 μg/mL graphene/Au-NPs, 30 mM H_2O_2, and 0.5 mM TMB, unless otherwise stated.

even in biological complexes. Due to the fact that the signal transduction mechanism of our sensor was exclusively related to the target–probe interaction, we investigated whether the assay can determine target strands in the presence of other DNA sequences. The result for mixtures of HCV-1a and HCV-6a with various fractions of target HCV-1b revealed that the assay was not able to distinguish the color signal from the background in the case of 40% target in the HCV cDNA mixtures (Figure S16B), possibly a result from the deactivation effect of adsorbed noncomplementary DNA. To address the critical issue in the analysis of HCV-1b, we performed a "back-mixing" protocol; that is, we first mixed the amount of catalyst with real HCV cDNA sample (containing HCV-1a, HCV-6a, and target HCV-1b) and ascertained that all of the HCV cDNA adequately adsorbed at the surface of graphene/Au-NPs. In this case, the catalytic activity was allowed to be switched off. In contrast, HCV-1b cDNA was more likely to be detached from the catalyst surface with increasing the amounts of probe HCV DNA until the ratio of probe to target reached 1 in theory, thus switching on the catalysis. As illustrated in Figure 5A, the graphene/Au-NP hybrid at a final concentration of 5 μg/mL was sufficient to accommodate HCV cDNA (total final concentration of 1.0 μM, containing 0.4 μM HCV-1b cDNA) derived from the negligible signal response in serum media. In the presence of a probe, the color signal increased notably with each incremental addition of HCV DNA until the concentration reached 0.5 μM (Figure 5B). Note that the hybridization reaction could be done well under optimal condition, thus it was possible to employ the back-mixing protocol to determine the amount of target quantitatively even in the presence of other nucleic acids. Furthermore, the current assay can be exploited to identify PCR-amplified DNA sequences where primers and other DNA fragments are present. Our future work will be focused on adapting the presented protocol for HCV detection in combination with reverse transcriptase reaction and polymerase chain reaction (PCR) amplification in real samples from sera patients.

Considering the fact that aptamers were triggered to undergo conformation changes upon the target binding,[17] we applied the tunable smart interface to construct a label-free aptamer-based sensing system. An intact anti-insulin aptamer without any labeling or modification was employed to evaluate the feasibility of the catalyst in aptamer-based assay.[69] We anticipated that the presence of target was necessary to induce the formation of an insulin/aptamer complex by means of specific binding reaction, which was then released from the catalyst surface, thus giving rise to a recovered active interface. Upon the addition of the TMB substrate, it was found that the color signal at 652 nm increased with the concentration of target insulin in the range of 0–600 nM (Figure S17). In a control experiment, no obvious color reaction was observed in the absence of target or the presence of other interferential proteins, such as human IgG, bovine serum albumin (BSA), and α-fetoprotein (AFP) (Figure S18), indicating the success of our approach. Moreover, this strategy can in principle facilitate the design of other label-free aptamer-based sensors for a wide range of analytes.

It was well-known that ssDNA adsorbed on graphene or the Au-NP surface with an affinity that depended on base length,[20,64,70] which, in turn, would result in length-dependent catalytic activity of the graphene/Au-NPs/ssDNA complex. To verify this hypothesis, the peroxidase-like activity of our catalyst upon exposure to ssDNA with different lengths (varying from 12- to 37-mer) was investigated. One observed that longer ssDNA showed higher inhibition effect on the interfacial catalytic reactions (Figure 5C), thereby offering a basis for colorimetric sensing nuclease activity. To demonstrate its potential application, S1 nuclease, a ssDNA-specific nuclease that can catalyze the cleavage of ssDNA to yield small mono- or oligonucleotide fragments,[71] was chosen as the model. Initially, the capturing ssDNA (37-mer) and the graphene/Au-NPs formed a self-assembled complex *via* π-stacking interactions,[63] facilitating the following complete inhibition on the reaction. Conversely, when the ssDNA substrate was cleaved by S1 nuclease into small fragments, the catalytic reaction could be switched on due to a relatively weak inhibition effect of short ssDNA. Therefore, the corresponding color-generating reaction associated with ssDNA cleavage process can be used to assay nuclease activity. Kinetic studies of the color changes in the presence of various S1 nuclease concentrations from 1.0 × 10^{-3} to 1.2 × 10^{-2} U/μL were carried out (Figure S19). Upon increasing the concentration of S1 nuclease, the color intensity was gradually increased. Direct evidence to confirm the cleavage of ssDNA was provided by gel electrophoresis (Figure S20). No band was observed for the ssDNA (37-mer) upon treatment with S1 nuclease for 20 min at 37 °C, indicating the effective cleavage reaction. Taken together, on the basis of the remarkable difference in the catalytic activity of the graphene/Au-NP hybrid with ssDNA containing different lengths, it was possible to construct a colorimetric sensing system for the nuclease activity.

CONCLUSION

In conclusion, by directly and selectively growing "naked" Au-NPs on graphene oxide to form the synergistic graphene/Au-NP hybrid, we have obtained a tunable graphene-based smart interface that exhibits an excellent switchable peroxidase-like activity in response to specific DNA molecules. The change in interfacial catalytic behavior is accompanied by surface-absorbed ssDNA molecules undergoing conformational transitions, which provides a powerful and versatile basis for novel graphene/aptamer-based colorimetric biosensors. It is worth noting that the present strategy possesses unique advantages that are not available in traditional graphene/aptamer-based systems. First of all, taking advantage of this novel signaling strategy, one could successfully avoid labeled or modified aptamer, which will simplify the experimental procedures and reduce the cost in the following applications. What is more, it should be beneficial to preserve the affinity and specificity of receptors. Second, such a reversible switching interface could be regarded as an ideal signal reporter with low background signal due to the "off–on" switching mode in the sensing. Finally, this convenient approach can be applicable to the other extended graphene/DNA-based systems for colorimetric detection of a broad range of analytes. We envision that the engineered catalytic graphene-based material could find its potential applications in the development of biocatalysis, bioassays, and smart material devices in the future.

MATERIALS AND METHODS

Chemicals and Reagents. Graphite powder (≤300 mesh) was obtained from Beijing Chemical Reagents Company. 2,2′-Azinobis-(3-ethylbenzothiozoline-6-sulfonic acid) diammonium salt (ABTS) was purchased from J&K Scientific Ltd. 3,3′,5,5′-Tetramethylbenzidine (TMB) was obtained from Sinopharm Chemical Reagent Co., Ltd. (Shanghai, China). Horseradish peroxidase (HRP) (≥250 U/mg) was purchased from Amresco (USA). Human IgG, bovine serum albumin (BSA), and α-fetoprotein (AFP) were provided by Beijing Wanyumeilan Scientific Inc. Insulin (27 U/mg) was obtained from Shanghai Yansheng Biochemical Reagent Co., Ltd. Other reagents were all analytical grade and purchased from Tianjin Kemiou Chemical Reagent Co., Ltd. DNA oligomers and S1 nuclease (160 U/μL, in 10 mM CH_3COONa, 150 mM NaCl, 0.05 mM $ZnSO_4$, and 50% glycerol, pH 4.6) were purchased from Takara Biotechnology Co. (Dalian, China). All DNA oligomers were purified by high-performance liquid chromatography (HPLC) (as shown in Table S1). Ultrapure water obtained from a Millipore water purification system (resistivity >18.0 MΩ cm^{-1}, Laikie Instrument Co., Ltd., Shanghai, China) was used throughout the experiments. All glassware was first cleaned with a mixture of HCl and HNO_3 (ratio of HCl/HNO_3 = 3:1 in volume) and thoroughly rinsed with ultrapure water. Phosphate buffer solution (PBS, 20 mM) with various pH values was prepared by mixing the stock solution of Na_2HPO_4 and NaH_2PO_4.

Instruments. FL measurements were performed using a Hitachi F-4500 spectrofluorimeter with a scan rate at 1200 nm/min. The photomultiplier tube (PMT) voltage was 700 V. The slits for excitation and emission were set at 5 nm/5 nm. UV–visible absorption spectra were recorded on a Jasco V-550 spectrometer. Atomic force microscopy (AFM) measurements were carried out on Agilent PicoPlus II. Low-magnification and high-magnification TEM images were carried out on a FEI Tecnai G^2 Spirit and FEI Tecnai G^2 F30 S-Twin transmission electron microscope, respectively. X-ray diffractometry (XRD) was performed on Shimadzu LabX XRD-6000 with Cu Kα radiation. The Raman spectra were recorded on a Renishaw Micro-Raman system 2000 spectrometer with He–Ne laser excitation (wavelength 623.8 nm). The reactive oxygen species •OH was detected using a Bruker Elexsys A200 electron spin resonance spectrometer (ESR, Bruker, Germany) with a 100 W short arc mercury lamp (ER 203UV system) as the irradiation light source. Electrochemical measurements were performed with a CHI 650B electrochemical analyzer (CH Instruments, Inc., Shanghai). X-ray photoelectron spectroscopy (XPS) was performed with a VG ESCALAB 250 spectrometer using a nonmonochromatized Al KR X-ray source (1486.6 eV).

Fluorescent Assay for ssDNA or dsDNA Binding. In a typical experiment, 3.5 μg/mL of graphene/Au-NPs and 0.5 μM DNA (FAM-labeled P1 or dsDNA) were added to 20 mM PBS buffer (pH 7.4) for time-dependent fluorescence measurement at $\lambda_{ex}/\lambda_{em}$ = 494/518 nm. The final volume of the solution was fixed at 500 μL. All of the experiments were performed at room temperature.

Catalytic Activity Inhibition Assay. Graphene/Au-NPs (8 μg/mL) were first mixed with different concentrations of P1 or dsDNA in 10 mM PBS buffer (pH 7.4). After 20 min reaction, the solution was transferred to a quartz cell containing 20 mM PBS buffer (pH 4.0) at room temperature. Subsequently, 30 mM H_2O_2, 0.5 mM TMB, or 5 mM ABTS was added to the mixtures for time-dependent absorbance measurement.

Label-Free Colorimetric Assay for DNA Sequence. The unlabeled probe P1 (1 μM) was hybridized with its complementary target T1 or single-base mismatched target (G was mutated to T, A, or C) with specific concentration in 20 mM PBS buffer (pH 7.4, containing 50 mM NaCl) under the following conditions: 10 cycles of 95 °C for 60 s and 25 °C for 120 s. After being cooled to room temperature, the graphene/Au-NPs were quickly added to the mixtures to a final concentration of 8 μg/mL and incubated at room temperature for 20 min. Then the solution was transferred to a quartz cell containing 20 mM PBS buffer (pH 4.0). Subsequently, H_2O_2 and TMB were added to final concentrations of 30 and 0.5 mM, respectively. The time-dependent absorbance measurements were then recorded at room temperature.

Electrophoresis Analysis. ssDNA (37-mer) before and after cleavage by S1 nuclease was loaded on loading buffer containing 30 mM EDTA, 36% (v/v) glycerol, 0.05% (w/v) xylene cyanol FF, and 0.05% (w/v) bromophenol blue, pH 7.0. The samples were then put on a 20% polyacrylamide gel in a 1 × TAE buffer (40 mM Tris acetate, 2 mM EDTA, pH 8.5) followed by electrophoresis for 180 min at 60 V. After ethidium bromide staining, the gel was imaged using a G:BOX HR system (Gene Co., Ltd.).

Conflict of Interest: The authors declare no competing financial interest.

Acknowledgment. This work was supported by the National Basic Research Program of China (2011CB936002), the Fundamental Research Funds for the Central Universities (DUT 10ZD115), and Program for Changjiang Scholars and Innovative Research Team in University (IRT0813).

Supporting Information Available: Preparation of graphene oxide (GO), graphene/Au-NP hybrids, graphene, and free Au-NPs; sample preparation for AFM, TEM, XRD, and Raman; preparation of dsDNA; label-free colorimetric assay for insulin and S1 nuclease activity; additional figures. This material is available free of charge *via* the Internet at http://pubs.acs.org.

REFERENCES AND NOTES

1. Novoselov, K. S.; Geim, A. K.; Morozov, S. V.; Jiang, D.; Zhang, Y.; Dubonos, S. V.; Grigorieva, I. V.; Firsov, A. A. Electric Field Effect in Atomically Thin Carbon Films. *Science* **2004**, *306*, 666–669.
2. Geim, A. K.; Novoselov, K. S. The Rise of Graphene. *Nat. Mater.* **2007**, *6*, 183–191.
3. Nair, R. R.; Blake, P.; Grigorenko, A. N.; Novoselov, K. S.; Booth, T. J.; Stauber, T.; Peres, N. M. R.; Geim, A. K. Fine Structure Constant Defines Visual Transparency of Graphene. *Science* **2008**, *320*, 1308.
4. Dikin, D. A.; Stankovich, S.; Zimney, E. J.; Piner, R. D.; Dommett, G. H. B.; Evmenenko, G.; Nguyen, S. T.; Ruoff, R. S. Preparation and Characterization of Graphene Oxide Paper. *Nature* **2007**, *448*, 457–460.
5. Zhu, Y. W.; Murali, S.; Cai, W. W.; Li, X. S.; Suk, J. W.; Potts, J. R.; Ruoff, R. S. Graphene and Graphene Oxide: Synthesis, Properties, and Applications. *Adv. Mater.* **2010**, *22*, 3906–3924.
6. Pumera, M. Graphene in Biosensing. *Mater. Today* **2011**, *14*, 308–315.
7. Shan, C.; Yang, H.; Song, J.; Han, D.; Ivaska, A.; Niu, L. Direct Electrochemistry of Glucose Oxidase and Biosensing for Glucose Based on Graphene. *Anal. Chem.* **2009**, *81*, 2378–2382.
8. Mohanty, N.; Berry, V. Graphene-Based Single-Bacterium Resolution Biodevice and DNA Transistor: Interfacing Graphene Derivatives with Nanoscale and Microscale Biocomponents. *Nano Lett.* **2008**, *8*, 4469–4476.
9. Ang, P. K.; Chen, W.; Wee, A. T. S.; Loh, K. P. Solution-Gated Epitaxial Graphene as pH Sensor. *J. Am. Chem. Soc.* **2008**, *130*, 14392–14393.
10. Ren, W.; Fang, Y.; Wang, E. A Binary Functional Substrate for Enrichment and Ultra-Sensitive SERS Spectroscopic Detection of Folic Acid Using Graphene Oxide/Ag Nanoparticles Hybrids. *ACS Nano* **2011**, *5*, 6425–6433.
11. Jung, J. H.; Cheon, D. S.; Liu, F.; Lee, K. B.; Seo, T. S. A Graphene Oxide Based Immuno-Biosensor for Pathogen Detection. *Angew. Chem., Int. Ed.* **2010**, *49*, 5708–5711.
12. Bai, L.; Yuan, R.; Chai, Y.; Zhuo, Y.; Yuan, Y.; Wang, Y. Simultaneous Electrochemical Detection of Multiple Analytes Based on Dual Signal Amplification of Single-Walled Carbon Nanotubes and Multi-Labeled Graphene Sheets. *Biomaterials* **2012**, *33*, 1090–1096.
13. Lin, L.; Liu, Y.; Tang, L.; Li., J. Electrochemical DNA Sensor by the Assembly of Graphene and DNA-Conjugated Gold Nanoparticles with Silver Enhancement Strategy. *Analyst* **2011**, *136*, 4732–4737.
14. Liu, F.; Piao, Y.; Choi, K. S.; Seo, T. S. Fabrication of Free-Standing Graphene Composite Films as Electrochemical Biosensors. *Carbon* **2012**, *50*, 123–133.
15. Pruneanu, S.; Pogacean, F.; Biris, A. R.; Ardelean, S.; Canpean, V.; Blanita, G.; Dervishi, E.; Biris, A. S. Novel Graphene−Gold Nanoparticle Modified Electrodes for the High Sensitivity Electrochemical Spectroscopy Detection and Analysis of Carbamazepine. *J. Phys. Chem. C* **2011**, *115*, 23387–23394.
16. Ellington, A. D.; Szostak, J. W. *In Vitro* Selection of RNA Molecules That Bind Specific Ligands. *Nature* **1990**, *346*, 818–822.
17. Liu, J.; Cao, Z.; Lu, Y. Functional Nucleic Acid Sensors. *Chem. Rev.* **2009**, *109*, 1948–1998.
18. Lu, C. H.; Yang, H. H.; Zhu, C. L.; Chen, X.; Chen, G. N. A Graphene Platform for Sensing Biomolecules. *Angew. Chem., Int. Ed.* **2009**, *48*, 4785–4787.
19. Chang, H.; Tang, L.; Wang, Y.; Jiang, J.; Li, J. Graphene Fluorescence Resonance Energy Transfer Aptasensor for the Thrombin Detection. *Anal. Chem.* **2010**, *82*, 2341–2346.
20. He, S.; Song, B.; Li, D.; Zhu, C.; Qi, W.; Wen, Y.; Wang, L.; Song, S.; Fang, H.; Fan, C. A Graphene Nanoprobe for Rapid, Sensitive, and Multicolor Fluorescent DNA Analysis. *Adv. Funct. Mater.* **2010**, *20*, 453–459.
21. Wang, Y.; Li, Z. H.; Hu, D. H.; Lin, C. T.; Li, J. H.; Lin, Y. H. Aptamer/Graphene Oxide Nanocomplex for *In Situ* Molecular Probing in Living Cells. *J. Am. Chem. Soc.* **2010**, *132*, 9274–9276.
22. Dong, H.; Gao, W. C.; Yan, F.; Ji, H.; Ju, H. Fluorescence Resonance Energy Transfer between Quantum Dots and Graphene Oxide for Sensing Biomolecules. *Anal. Chem.* **2010**, *82*, 5511–5517.
23. Liu, M.; Zhao, H. M.; Quan, X.; Chen, S.; Fan, X. F. Distance-Independent Quenching of Quantum Dots by Nanoscale-Graphene in Self-Assembled Sandwich Immunoassay. *Chem. Commun.* **2010**, *46*, 7909–7911.
24. Wang, L.; Pu, K.; Li, J.; Qi, X.; Li, H.; Zhang, H.; Fan, C.; Liu, B. A Graphene-Conjugated Oligomer Hybrid Probe for Light-Up Sensing of Lectin and *Escherichia coli*. *Adv. Mater.* **2011**, *23*, 4386–4391.
25. Tang, D.; Tang, J.; Li, Q.; Su, B.; Chen, G. N. Ultrasensitive Aptamer-Based Multiplexed Electrochemical Detection by Coupling Distinguishable Signal Tags with Catalytic Recycling of DNase I. *Anal. Chem.* **2011**, *83*, 7255–7259.
26. Gulbakan, B.; Yasun, E.; Shukoor, M. I.; Zhu, Z.; You, M.; Tan, X.; Sanchez, H.; Powell, D. H.; Dai, H.; Tan, W. A Dual Platform for Selective Analyte Enrichment and Ionization in Mass Spectrometry Using Aptamer-Conjugated Graphene Oxide. *J. Am. Chem. Soc.* **2010**, *132*, 17408–17410.
27. Guo, S.; Du, Y.; Yang, X.; Dong, S.; Wang, E. Solid-State Label-Free Integrated Aptasensor Based on Graphene-Mesoporous Silica-Gold Nanoparticle Hybrids and Silver Microspheres. *Anal. Chem.* **2011**, *83*, 8035–8040.
28. Ohno, Y.; Maehashi, K.; Matsumoto, K. Label-Free Biosensors Based on Aptamer-Modified Graphene Field-Effect Transistors. *J. Am. Chem. Soc.* **2010**, *132*, 18012–18013.
29. Zhang, X.; Li, S.; Jin, X.; Zhang, S. A New Photoelectrochemical Aptasensor for the Detection of Thrombin Based on Functionalized Graphene and CdSe Nanoparticles Multilayers. *Chem. Commun.* **2011**, *47*, 4929–4931.
30. Xiang, Y.; Yong, A.; Lu, Y. Abasic Site-Containing DNAzyme and Aptamer for Label-Free Fluorescent Detection of Pb^{2+} and Adenosine with High Sensitivity, Selectivity, and Tunable Dynamic Range. *J. Am. Chem. Soc.* **2009**, *131*, 15352–15357.
31. Wang, Y.; Li, J.; Jin, J.; Wang, H.; Tang, H.; Yang, R.; Wang, K. Strategy for Molecular Beacon Binding Readout: Separating Molecular Recognition Element and Signal Reporter. *Anal. Chem.* **2009**, *81*, 9703–9709.
32. Balapanuru, J.; Yang, J. X.; Xiao, S.; Bao, Q. L.; Jahan, M.; Polavarapu, L.; Wei, J.; Xu, Q. H.; Loh, K. P. A Graphene Oxide−Organic Dye Ionic Complex with DNA-Sensing and Optical-Limiting Properties. *Angew. Chem., Int. Ed.* **2010**, *49*, 6549–6553.
33. Liu, M.; Zhao, H. M.; Chen, S.; Yu, H. T.; Zhang, Y. B.; Quan, X. Label-Free Fluorescent Detection of Cu(II) Ions Based on DNA Cleavage-Dependent Graphene-Quenched DNAzymes. *Chem. Commun.* **2011**, *47*, 7749–7751.

34. Cai, L.; Zhan, R.; Pu, K.; Qi, X.; Zhang, H.; Huang, W.; Liu, B. Butterfly-Shaped Conjugated Oligoelectrolyte/Graphene Oxide Integrated Assay for Light-Up Visual Detection of Heparin. *Anal. Chem.* **2011**, *83*, 7849–7855.
35. Bonanni, A.; Pumera, M. Graphene Platform for Hairpin-DNA-Based Impedimetric Genosensing. *ACS Nano* **2011**, *5*, 2356–2361.
36. Wang, L.; Zhu, C.; Han, L.; Jin, L.; Zhou, M.; Dong, S. Label-Free, Regenerative and Sensitive Surface Plasmon Resonance and Electrochemical Aptasensors Based on Graphene. *Chem. Commun.* **2011**, *47*, 7794–7796.
37. Wang, H.; Cui, L. F.; Yang, Y.; Casalongue, H. S.; Robinson, J. T.; Liang, Y.; Cui, Y.; Dai, H. Mn_3O_4-Graphene Hybrid as a High-Capacity Anode Material for Lithium Ion Batteries. *J. Am. Chem. Soc.* **2010**, *132*, 13978–13980.
38. Zhou, Y.; Bao, Q. L.; Tang, A. L. L.; Zhong, Y. L.; Loh, K. P. Hydrothermal Dehydration for the "Green" Reduction of Exfoliated Graphene Oxide to Graphene and Demonstration of Tunable Optical Limiting Properties. *Chem. Mater.* **2009**, *21*, 2950–2956.
39. Yoo, E.; Okata, T.; Akita, T.; Kohyama, M.; Nakamura, J.; Honma, I. Enhanced Electrocatalytic Activity of Pt Subnanoclusters on Graphene Nanosheet Surface. *Nano Lett.* **2009**, *9*, 2255–2259.
40. Chen, X.; Wu, G.; Chen, J.; Chen, X.; Xie, Z.; Wang, X. Synthesis of "Clean" and Well-Dispersive Pd Nanoparticles with Excellent Electrocatalytic Property on Graphene Oxide. *J. Am. Chem. Soc.* **2011**, *133*, 3693–3695.
41. Jasuja, K.; Berry, V. Implantation and Growth of Dendritic Gold Nanostructures on Graphene Derivatives: Electrical Property Tailoring and Raman Enhancement. *ACS Nano* **2009**, *3*, 2358–2366.
42. Gao, L. Z.; Zhuang, J.; Nie, L.; Zhang, J. B.; Zhang, Y.; Gu, N.; Wang, T. H.; Feng, J.; Yang, D. L.; Perrett, S.; Yan, X. Y. Intrinsic Peroxidase-like Activity of Ferromagnetic Nanoparticles. *Nat. Nanotechnol.* **2007**, *2*, 577–583.
43. Song, Y.; Qu, K.; Zhao, C.; Ren, J.; Qu, X. Graphene Oxide: Intrinsic Peroxidase Catalytic Activity and Its Application to Glucose Detection. *Adv. Mater.* **2010**, *22*, 2206–2210.
44. He, W.; Liu, Y.; Yuan, J.; Yin, J.; Wu, X.; Hu, X.; Zhang, K.; Liu, J.; Chen, C.; Ji, Y.; Guo, Y. Au@Pt Nanostructures as Oxidase and Peroxidase Mimetics for Use in Immunoassays. *Biomaterials* **2011**, *32*, 1139–1147.
45. Wang, X.; Qu, K.; Xu, B.; Ren, J.; Qu, X. Multicolor Luminescent Carbon Nanoparticles: Synthesis, Supramolecular Assembly with Porphyrin, Intrinsic Peroxidase-like Catalytic Activity and Applications. *Nano Res.* **2011**, *4*, 908–920.
46. Liang, Y.; Li, Y.; Wang, H.; Zhou, J.; Wang, J.; Regier, T.; Dai, H. Co_3O_4 Nanocrystals on Graphene as a Synergistic Catalyst for Oxygen Reduction Reaction. *Nat. Mater.* **2011**, *10*, 780–786.
47. Guo, Y.; Deng, L.; Li, J.; Guo, S.; Wang, E.; Dong, S. Hemin–Graphene Hybrid Nanosheets with Intrinsic Peroxidase-like Activity for Label-Free Colorimetric Detection of Single-Nucleotide Polymorphism. *ACS Nano* **2011**, *5*, 1282–1290.
48. Johari, P.; Shenoy, V. B. Modulating Optical Properties of Graphene Oxide: Role of Prominent Functional Groups. *ACS Nano* **2011**, *5*, 7640–7647.
49. Luque, G. L.; Rojasa, M. I.; Rivas, G. A.; Leiva, E. P. M. The Origin of the Catalysis of Hydrogen Peroxide Reduction by Functionalized Graphene Surfaces: A Density Functional Theory Study. *Electrochim. Acta* **2010**, *56*, 523–530.
50. Ran, Q.; Gao, M.; Guan, X.; Wang, Y.; Yu, Z. First-Principles Investigation on Bonding Formation and Electronic Structure of Metal–Graphene Contacts. *Appl. Phys. Lett.* **2009**, *94*, 103511.
51. Zhou, M.; Zhang, A.; Dai, Z.; Zhang, C.; Feng, Y. P. Greatly Enhanced Adsorption and Catalytic Activity of Au and Pt Clusters on Defective Graphene. *J. Chem. Phys.* **2010**, *132*, 194704.
52. Zhang, Z.; Berg, A.; Levanon, H.; Fessenden, R. W.; Meisel, D. On the Interactions of Free Radicals with Gold Nanoparticles. *J. Am. Chem. Soc.* **2003**, *125*, 7959–7963.
53. Giovannetti, G.; Khomyakov, P. A.; Brocks, G.; Karpan, V. M.; Brink, J.; Kelly, P. J. Doping Graphene with Metal Contacts. *Phys. Rev. Lett.* **2008**, *101*, 026803.
54. Sundaram, R. S.; Steiner, M.; Chiu, H. Y.; Engel, M.; Bol, A. A.; Krupke, R.; Burghard, M.; Kern, K.; Avouris, P. The Graphene–Gold Interface and Its Implications for Nanoelectronics. *Nano Lett.* **2011**, *11*, 3833–3837.
55. Das, A.; Pisana, S.; Chakraborty, B.; Piscanec, S.; Saha, S. K.; Waghmare, U. V.; Novoslov, K. S.; Krishnamurthy, H. R.; Geim, A. K.; Ferrari, A. C.; Sood, A. K. Monitoring Dopants by Raman Scattering in an Electrochemically Top-Gated Graphene Transistor. *Nat. Nanotechnol.* **2008**, *3*, 210–215.
56. Lee, J.; Novoselov, K. S.; Shin, H. S. Interaction between Metal and Graphene: Dependence on the Layer Number of Graphene. *ACS Nano* **2011**, *5*, 608–612.
57. Lin, Y. C.; Lin, C. Y.; Chiu, P. W. Controllable Graphene N-Doping with Ammonia Plasma. *Appl. Phys. Lett.* **2010**, *96*, 133110.
58. Huh, S.; Park, J.; Kim, K. S.; Hong, B. H.; Kim, S. B. Selective n-Type Doping of Graphene by Photo-Patterned Gold Nanoparticles. *ACS Nano* **2011**, *5*, 3639–3644.
59. Pinto, H.; Jones, R.; Goss, J. P.; Briddon, P. R. Mechanisms of Doping Graphene. *Phys. Status Solidi A* **2010**, *207*, 2131–2136.
60. Subrahmanyam, K. S.; Manna, A. K.; Pati, S. K.; Rao, C. N. R. A Study of Graphene Decorated with Metal Nanoparticles. *Chem. Phys. Lett.* **2010**, *497*, 70–75.
61. Tang, Y.; Allen, B. L.; Kauffman, D. R.; Star, A. Electrocatalytic Activity of Nitrogen-Doped Carbon Nanotube Cups. *J. Am. Chem. Soc.* **2009**, *131*, 13200–13201.
62. Lu, Y. H.; Zhou, M.; Zhang, C.; Feng, Y. P. Metal-Embedded Graphene: A Possible Catalyst with High Activity. *J. Phys. Chem. C* **2009**, *113*, 20156–20160.
63. Varghese, N.; Mogera, U.; Govindaraj, A.; Das, A.; Maiti, P. K.; Sood, A. K.; Rao, C. N. R. Binding of DNA Nucleobases and Nucleosides with Graphene. *ChemPhysChem* **2009**, *10*, 306–210.
64. Li, H.; Rothberg, L. J. Label-Free Colorimetric Detection of Specific Sequences in Genomic DNA Amplified by the Polymerase Chain Reaction. *J. Am. Chem. Soc.* **2004**, *126*, 10958–10961.
65. Swathi, R. S.; Sebastian, K. L. Resonance Energy Transfer from a Dye Molecule to Graphene. *J. Chem. Phys.* **2008**, *129*, 054703.
66. Gaylord, B. S.; Heeger, A. J.; Bazan, G. C. DNA Hybridization Detection with Water-Soluble Conjugated Polymers and Chromophore-Labeled Single-Stranded DNA. *J. Am. Chem. Soc.* **2003**, *125*, 896–900.
67. Syvanen, A. C. Accessing Genetic Variation: Genotyping Single Nucleotide Polymorphisms. *Nat. Rev. Genet.* **2001**, *2*, 930–942.
68. Liu, S.; Wu, P.; Li, W.; Zhang, H.; Cai, C. Ultrasensitive and Selective Electrochemical Identification of Hepatitis C Virus Genotype 1b Based on Specific Endonuclease Combined with Gold Nanoparticles Signal Amplification. *Anal. Chem.* **2011**, *83*, 4752–4758.
69. Yoshida, W.; Mochizuki, E.; Takase, M.; Hasegawa, H.; Morita, Y.; Yamazaki, H.; Sode, K.; Ikebukuro, K. Selection of DNA Aptamers Against Insulin and Construction of an Aptameric Enzyme Subunit for Insulin Sensing. *Biosens. Bioelectron.* **2009**, *24*, 1116–1120.
70. Zhao, X.; Kong, R.; Zhang, X.; Meng, H.; Liu, W.; Tan, W.; Shen, G.; Yu, R. Graphene-DNAzyme Based Biosensor for Amplified Fluorescence "Turn-On" Detection of Pb^{2+} with a High Selectivity. *Anal. Chem.* **2011**, *83*, 5062–5066.
71. Tang, Y. L.; Feng, F. D.; He, F.; Wang, S.; Li, Y. L.; Zhu, D. B. Direct Visualization of Enzymatic Cleavage and Oxidative Damage by Hydroxyl Radicals of Single-Stranded DNA with a Cationic Polythiophene Derivative. *J. Am. Chem. Soc.* **2006**, *128*, 14972–14976.